NEOPLASIA
www.neoplasia.com

Volume 21 Number 2 February 2019 pp. 239–246 239

Hypoxia Patterns in Primary and Metastatic Prostate Cancer Environments[1]

Santosh Kumar Bharti[*], Samata Kakkad[*], Pierre Danhier[*,2], Flonne Wildes[*], Marie-France Penet[*,†], Balaji Krishnamachary[*] and Zaver M. Bhujwalla[*,†,‡]

[*]Division of Cancer Imaging Research, The Russell H. Morgan Department of Radiology and Radiological Science, The Johns Hopkins University School of Medicine, Baltimore, MD, USA; [†]Sidney Kimmel Comprehensive Cancer Center, The Johns Hopkins University School of Medicine; Baltimore, MD, USA; [‡]Radiation Oncology and Molecular Radiation Sciences, The Johns Hopkins University School of Medicine, Baltimore, MD, USA

Abstract

Metastatic dissemination continues to be a major cause of prostate cancer (PCa) mortality, creating a compelling need to understand factors that play a role in the metastatic cascade. Since hypoxia plays an important role in PCa aggressiveness, we characterized patterns of hypoxia in the primary tumor and metastatic environments of a human PCa xenograft. We previously developed and characterized an imaging strategy based on the hypoxia response element (HRE)–driven expression of long-lived enhanced green fluorescent protein (EGFP) and short-lived luciferase (luc) fused to the oxygen-dependent degradation domain in human PCa PC-3 cells. Both reporter proteins were placed under the transcriptional control of a five–tandem repeat HRE sequence. PC-3 cells also constitutively expressed the tdTomato red fluorescent protein, allowing cancer cell detection *in vivo*. This "timer" strategy can provide information on the temporal evolution of HIF activity and hypoxia in tumors. Here, for the first time, we performed *in vivo* and *ex vivo* imaging of this dual HIF reporter system in PC-3 metastatic tumors implanted orthotopically in the prostate and PC-3 nonmetastatic tumors implanted subcutaneously. We observed distinct patterns of EGFP and luc expression in subcutaneous and orthotopic tumors, and in metastatic nodules, that provide new insights into the presence of hypoxia at primary and metastatic tumor sites, and of the role of hypoxia in metastasis.

Neoplasia (2019) 21, 239–246

Introduction

Hypoxia contributes to aggressiveness, resistance to treatment, and metastatic dissemination of cancer [1–4]. Prostate cancer (PCa) ranks high among the malignancies in which hypoxia plays a major role in treatment resistance and metastases [5,6]. In PCa, hypoxia associated gene expression of lysyl oxidase and glucose transporter-1 (GLUT-1) has been correlated with Gleason score [7]. More recently, carbonic anhydrase (CA) IX, another hypoxia regulated enzyme that plays a role in cytoplasmic pH regulation of cancer cells, was found to correlate with higher Gleason scores [8]. Hypoxia has also been implicated in the emergence of castration-resistant PCa cells [9]. In a large clinical study, PCa hypoxia was associated with early biochemical relapse after radiotherapy and with local recurrence [10]. In a separate retrospective analysis of two randomized

Abbreviations: BLI, bioluminescence imaging; EGFP, enhanced green fluorescent protein; HIF, hypoxia inducible factor; HRE, hypoxia response element; Luc, luciferase; ODD, oxygen-dependent degradation domain; PCa, prostate cancer; RFP, red fluorescent protein; SEM, standard error of the mean.

Address all correspondence to: Zaver M. Bhujwalla, PhD, The Johns Hopkins University School of Medicine, 208C Traylor Building, 720 Rutland Avenue, Baltimore, MD 21205, USA. E-mail: zaver@mri.jhu.edu

[1] Acknowledgement: This work was supported by National Institutes of Health R35 CA209960, R01 CA73850, R01 CA82337, and P30 CA006973.

[2] Current address: Louvain Drug Research Institute, Nuclear and Electron Spin Technologies (NEST) Platform, Université catholique de Louvain (UCL), Brussels, Belgium.

Received 11 October 2018; Revised 12 December 2018; Accepted 13 December 2018

1476-5586
https://doi.org/10.1016/j.neo.2018.12.004

radiotherapy trials and one surgical cohort study, increased staining of HIF-1α was a significant predictor of biochemical failure after radiotherapy or surgery [11]. In preclinical studies, prostate cancer models such as those developed from the Dunning prostate cancer model [12] at Johns Hopkins, [13] have been well characterized in terms of differences in patterns of vascularization, hypoxia, and radiation response [14–16].

Chronic hypoxia results from the limited diffusion of oxygen to tumor cells distant from blood vessels [17]. Acute hypoxia can result from vascular collapse due to increased tumor interstitial pressure [17]. The formation of hypoxia results in the upregulation of vascular endothelial growth factor [18] that can lead to increased angiogenesis and neovascularization and reoxygenation of hypoxic regions. Reoxygenation also occurs during therapy, or during tumor evolution, when cell death provides increased nutrients and oxygen to the remaining cells [14,19–21].

The adaptive response of cancer cells to hypoxia is mediated through the stabilization of hypoxia inducible factors (HIFs) that increases the transcription of several genes mediating this response by binding to hypoxia response elements (HREs) in the promoter region of these genes [5]. HIF is a heterodimeric basic helix-loop-helix PAS (Per-ARNT-Sim) domain containing transcription factor that consists of one of three oxygen-regulated α-subunits, HIF-1α, HIF-2α, and HIF-3α and a constitutively expressed β-subunit (HIF-β/ARNT) [22,23]. The α-subunits are constitutively transcribed and translated but are regulated at the protein level by oxygen-dependent hydroxylation of specific prolyl residues and degraded due to the presence of an oxygen-dependent degradation domain (ODD) [24].

There is a critical need to understand the metastatic cascade in PCa to design effective interventions to prevent metastasis and to identify markers of aggressiveness. We developed an HRE-driven imaging strategy that combines the hypoxia-driven expression of two optical reporters with different half-lives to detect temporal changes in hypoxia and HIF activity [25]. For this purpose, human PCa cells were transfected with the luciferase (luc) gene fused with an oxygen-dependent degradation domain (ODD-luc) and a variant of the enhanced green fluorescent protein (EGFP), both of which were driven by a five–tandem repeat HRE sequence (5xHRE). The cells constitutively expressed tdTomato red fluorescent protein (RFP) that was regulated by a phosphoglycerate kinase (pGK) promoter. This novel "timer" imaging strategy of combining the short-lived ODD-luc and the long-lived EGFP, provided a time frame of HRE activation in tumors derived from these PCa cells that was used, for the first time, to understand the relationship between temporal changes in hypoxia in primary and metastatic lesions. Since human cancer xenografts metastasize more readily from the orthotopic implantation site compared to a subcutaneous inoculation site [2,26,27], PC-3-HRE-EGFP/HRE-ODD-luc/tdTomato cells were inoculated subcutaneously or orthotopically in a group of mice to determine if differences in expression patterns of luc and EGFP were detected in primary tumors and metastatic lesions. By using this novel timer-reporter strategy, we characterized hypoxia patterns in human PCa xenografts and metastatic lesions that developed in tumor-bearing mice. With this timer strategy, regions with high bioluminescence (BL) but low EGFP may represent early or acute hypoxia, regions with high BL and high EGFP may represent long-term chronic hypoxia, and regions with low BL and high EGFP may represent reoxygenated regions that were previously hypoxic [25]. We detected significant differences in the patterns of expression of the timer-reporters between subcutaneous and orthotopic tumors and in the metastatic lesions that provide new insights into the development of hypoxia and its role in metastatic dissemination from these tumors.

Materials and Methods

Generation of PC3-HRE-EGFP/HRE-ODD-luc Cells

Detailed methods and validation of the system were previously reported [25]. Briefly, to construct the plasmid encoding the luc gene fused to ODD under the regulation of a five–tandem repeat of HRE sequence (5xHRE) with a puromycin resistance cassette, the *5xHRE-ODD-luc* (firefly luciferase fused with ODD) sequence from a 5HREp-ODD-luc plasmid (kindly provided by Dr. H. Harada) was digested with KpnI and XbaI and subcloned between KpnI and EcoRI of a pGL4.21 [luc2P/Puro] vector (Promega, Madison, WI). Human PCa PC-3 cells expressing EGFP variant pd2EGFP under the promotion of a 5xHRE sequence (PC3-HRE-EGFP) were transfected with the 5xHRE-ODD-luc construct (PC3-HRE-ODD-luc and PC3-HRE-EGFP/HRE-ODD-luc) using jetPRIME reagent (Polyplus transfection) following the manufacturer's protocol. Transfected cells were selected using 1 μg/ml of puromycin. PC3-HRE-EGFP/HRE-ODD-luc cells constitutively expressing the bright red fluorescent protein tdTomato (PC3-HRE-EGFP/HRE-ODD-luc/tdTomato) were generated by lentiviral infection with the pRRL-Δluc-tdtomato plasmid [25].

Cell Inoculation and Animal Studies

All experimental animal protocols and animal handling were performed in accordance with protocols approved by the Institutional Animal Care and Use Committee of the Johns Hopkins University School of Medicine and conformed to the Guide for the Care and Use of Laboratory Animals published by the National Institutes of Health. Male adult nude mice were inoculated subcutaneously with 2×10^6 cancer cells. For orthotopic implantation, a 1-mm^3 piece of tumor tissue obtained from a subcutaneous tumor was microsurgically sutured into the prostate gland through a small incision as previously described [27]. Tumor pieces used for implantation were carefully dissected under a fluorescence microscope to remove hypoxic and necrotic tissue. Subcutaneous (n = 3) and orthotopic (n = 5) tumor volumes, measured *ex vivo*, were approximately 450± 94 mm^3 and 720± 151 mm^3 [mean ± standard error of the mean (SEM)] respectively, at the time of imaging. There was no close association between tumor volume and metastatic dissemination.

In Vivo Optical Imaging

Optical imaging was performed using an IVIS Spectrum scanner (Caliper Life Sciences, Hopkinton, MA). EGFP was detected using an excitation light of 500 nm and an emission filter set at 540 nm. tdTomato was detected using an excitation light of 570 nm and an emission filter set at 620 nm as described earlier [25]. To detect the expression of luc *in vivo* with bioluminescent imaging (BLI), 100 μl of a 30 mg/ml solution of D-luciferin (Promega, P1042, VivoGlo Luciferin, *In Vivo* Grade, potassium salt) dissolved in PBS was injected intraperitoneally (~3 mg/mouse) 15 minutes prior to imaging. We used an exposure time of 1 second for GFP and tdTomato and 1 minute for BLI, with a 6.4×6.4-cm field of view.

Ex Vivo Optical Imaging

Endpoint optical imaging of fluorescence and BL of fresh 2-mm–thick tumor slices, prepared with a tissue slicer, was performed with the IVIS Spectrum scanner. To quantify fluorescence and BL in tissue

slices, 2-mm–thick tumor slices, obtained from the tumor after euthanization of mice following *in vivo* imaging, were imaged. We used an exposure time of 0.1-0.2 second for EGFP and tdTomato and 30 second-1 minute for BLI. The *ex vivo* image analyses were done on normalized images using the IVIS software.

Fluorescence and BL areas higher than 50% of the background were determined in the tumor slices using the Living Image software (Perkin Elmer, Waltham, MA) and normalized to the total area of each slice to obtain fractional areas of EGFP and BL.

Statistical Analyses

All results are represented as mean ± SEM. Comparisons between groups were performed using a two-tailed unpaired Student's *t* test. *P* values < .05 were considered to be statistically significant unless otherwise stated.

Results

Orthotopic tumors formed detectable metastatic lesions frequently, unlike the subcutaneous tumors (three of five mice with orthotopic tumors displayed metastasis, whereas none of the mice with subcutaneous tumors had detectable metastasis). Representative *in vivo* optical images of an orthotopic PC3-HRE-EGFP/HRE-ODD-luc/tdTomato tumor with a peritoneal metastatic lesion revealing patterns of luc and EGFP expression in primary and metastatic lesions are shown in Figure 1, *A-C*. Optical images from (A) tdTomato expression that identifies cancer cells, (B) HRE-driven EGFP expression, and (C) HRE-driven luc expression are displayed. The EGFP fluorescence and luc BL distributions demonstrate patterns of chronic and acute hypoxia in the primary and metastatic lesions. Here, the primary tumor had a small focus of EGFP expression indicative of long-term exposure to hypoxia that was also identified with BLI but within a smaller area, suggesting that the hypoxia may have been resolving. In contrast, there were areas of BL in the primary tumor and in the metastatic lesion that were not detected in the EGFP image that suggested that these regions were newly hypoxic.

We also observed examples of tumors where only BL was observed but not EGFP fluorescence, as shown in the representative examples of tdTomato, EGFP, and luc expression in Figure 2, *A-C* where, in this instance, hypoxia must have occurred within an 8-hour time frame that allowed expression of luc but not EGFP. In this mouse, we also observed a metastatic lesion expressing EGFP but not luc. The difference in BL intensities between Figures 1*C* and 2*C* was most likely because of differences in the amount of luciferin reaching the tumor.

Representative *ex vivo* images of a metastatic nodule in the liver formed from an orthotopic PC3-HRE-EGFP/HRE-ODD-luc/tdTomato tumor are displayed in Figure 3, *A-C*. Optical images from (A) tdTomato expression to identify cancer cells, (B) HRE-driven EGFP expression, and (C) HRE-driven luc expression are displayed. In this metastatic nodule, fluorescence from EGFP and BL from luc is observed in two distinct regions of the lesion identified by RFP expression. The EGFP fluorescing area without BL suggests that cells in this region were previously exposed to hypoxia, whereas the BL region without EGFP expression suggests that hypoxia must have occurred within the past 8 hours that allowed luc to be formed but not EFGP.

In Figure 4, *ex vivo* images of (A) tdTomato expression, (B) HRE-driven EGFP expression, and (C) HRE-driven luc expression in eight metastatic lesions obtained from a single mouse (Met 1 to Met 8) with an orthotopic PC3-HRE-EGFP/HRE-ODD-luc/tdTomato tumor are displayed together with (D) bar plots of the fractional area of EGFP and luc expression in these lesions. There is an overall trend towards higher EGFP and lower BL fractional areas in these metastatic lesions, suggesting that cancer cells in the metastatic lesions were exposed to hypoxia within the past 8-24 hours either at the

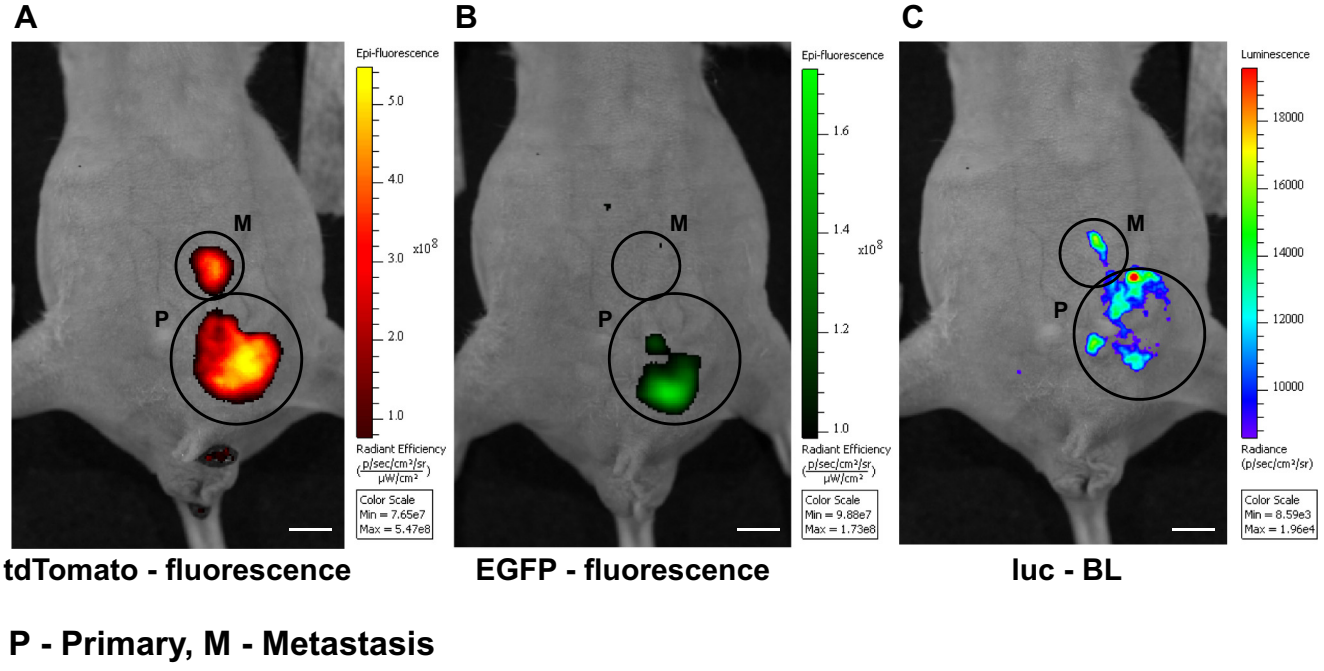

Figure 1. Representative *in vivo* optical images of an orthotopic PC3-HRE-EGFP/HRE-ODD-luc/tdTomato tumor-bearing mouse with a peritoneal metastatic lesion revealing patterns of EGFP and BL expression in primary and metastatic lesions. Optical images are from (A) tdTomato expression to identify cancer cells, (B) HRE-driven EGFP expression, and (C) HRE-driven luc expression. Scale bar: 0.5 cm.

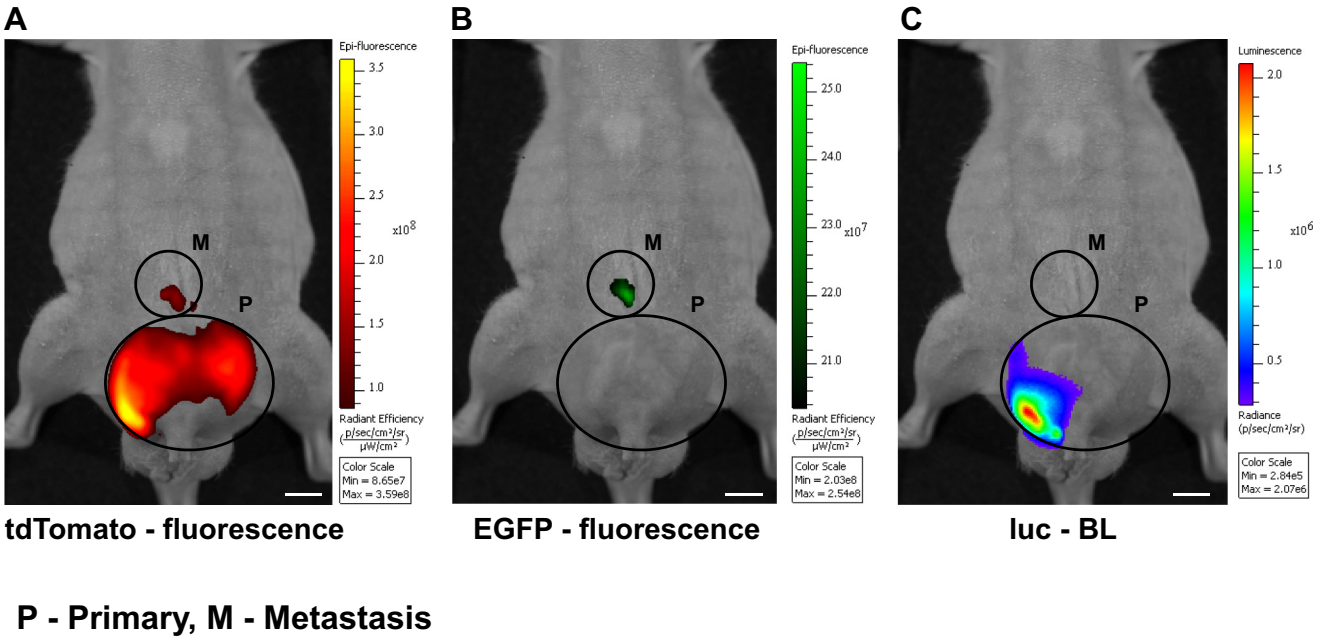

Figure 2. Representative *in vivo* optical images of an orthotopic PC3-HRE-EGFP/HRE-ODD-luc/tdTomato tumor-bearing mouse with extensive BL but no EGFP expression. Also observed is a small metastatic lesion that expresses EGFP fluorescence but not BL. Optical images are from (A) tdTomato expression to identify cancer cells, (B) HRE-driven EGFP expression, and (C) HRE-driven luc expression. Scale bar: 0.5 cm.

primary site or at the metastatic site but were not hypoxic in the metastatic lesion when imaged.

Representative images of tdTomato, EGFP, and luc expression from cancer cells in ascites fluid, obtained from the peritoneal cavity of a mouse with an orthotopic PC3-HRE-EGFP/HRE-ODD-luc/tdTomato tumor, are shown in Figure 5, *A-C*. Cancer cells in the ascites fluid expressed EGFP but not luc, suggesting that these cells were exposed to hypoxia within the past 8-24 hours but were not hypoxic when imaged.

Patterns of EGFP and BL obtained from *ex vivo* subcutaneous and orthotopic tumors, and *ex vivo* metastatic nodules are shown in Figure 6. Fractional areas of EGFP or BL were not significantly different between subcutaneous and orthotopic tumors. However, fractional areas of EGFP were significantly higher and fractional areas of BL were significantly lower in the metastatic lesions compared to subcutaneous and orthotopic tumors. These results suggest that cells in metastatic lesions had been previously exposed to hypoxia, either at the primary tumor site or at the metastatic site, but the hypoxia had resolved. Within each group, the EGFP fractional area was significantly higher than the BL area in orthotopic tumors and metastatic lesions but not in subcutaneous tumors.

Since BL depends on HRE-driven luc expression as well as the delivery of D-luciferin to the tumor, a PC3-HRE-EGFP/HRE-

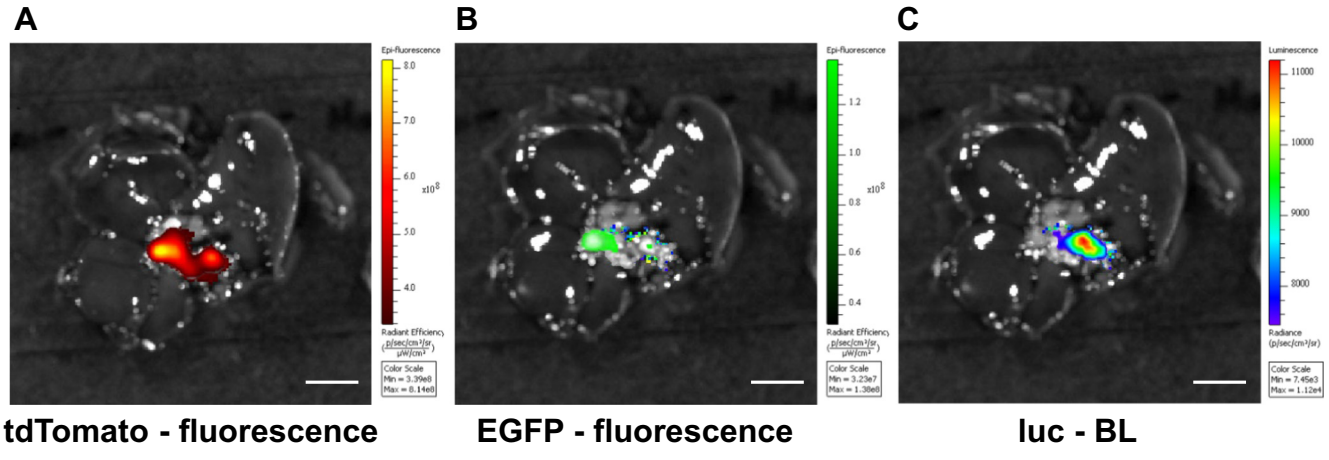

Figure 3. Representative *ex vivo* images of a metastatic nodule in the liver resulting from an orthotopic PC3-HRE-EGFP/HRE-ODD-luc/tdTomato tumor. Optical images are from (A) tdTomato expression to identify cancer cells, (B) HRE-driven EGFP expression, and (C) HRE-driven luc expression. In this metastatic nodule, the EGFP fluorescence and BL are observed in two distinct regions of the tumor. Scale bar: 0.5 cm.

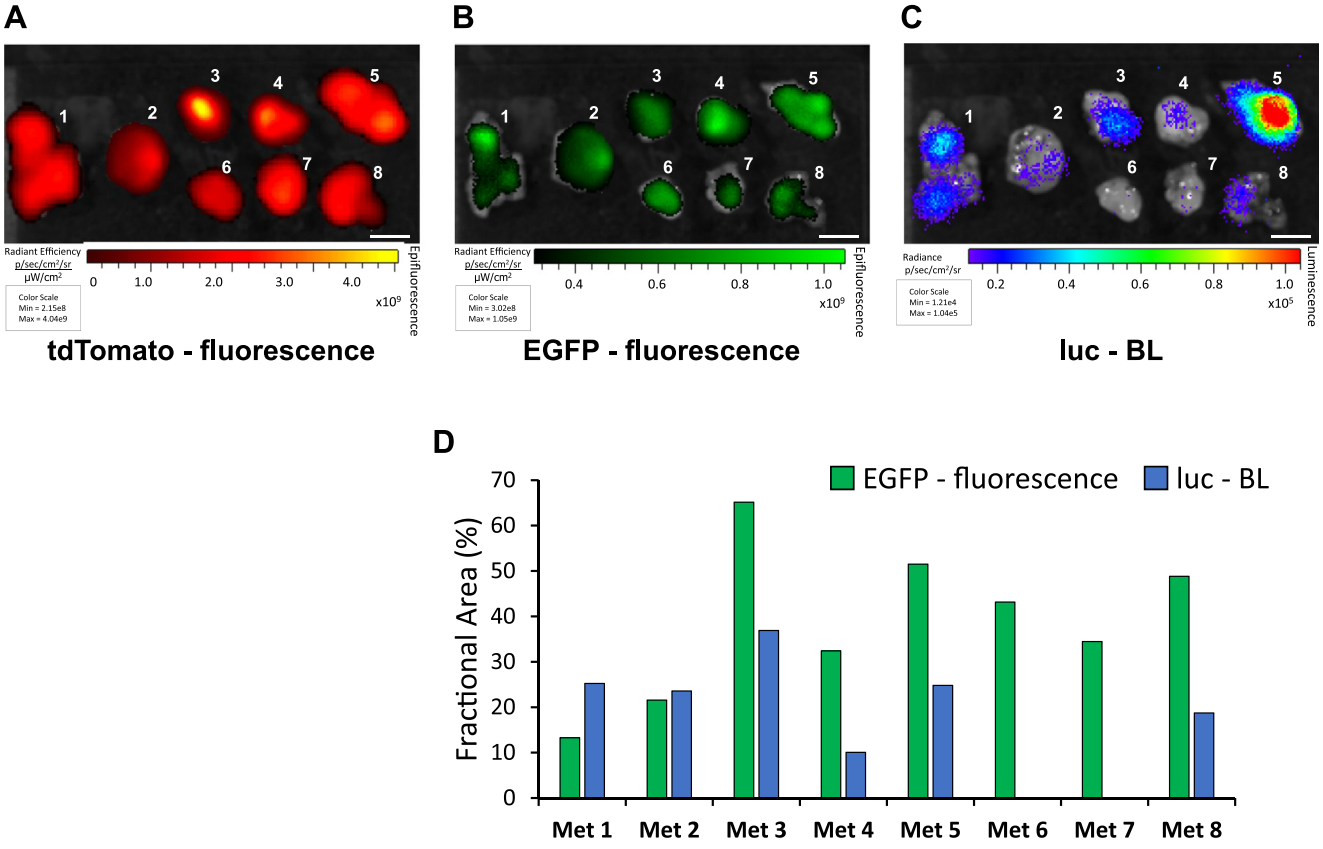

Figure 4. *Ex vivo* images of (A) tdTomato expression, (B) HRE-driven EGFP expression, and (C) HRE-driven luc expression in eight metastatic lesions (Met 1 to Met 8), obtained from a single mouse with an orthotopic PC3-HRE-EGFP/HRE-ODD-luc/tdTomato tumor, are displayed together with (D) bar plots of the fractional area of EGFP fluorescence and BL in these lesions. Scale bar: 0.5 cm.

ODD-luc tumor was imaged *ex vivo* immediately after *in vivo* imaging and reimaged after layering D-luciferin solution directly on the tumor slice. As shown in Supplementary Figure S1, layering D-luciferin on the tumor slice increased the BL signal intensity but did not reveal any additional BL areas, indicating effective delivery of D-luciferin within the tumor and the hypoxia dependence of BL.

Discussion

Our purpose in this study was to characterize hypoxic environments in primary and metastatic lesions to gain further insights into the role of hypoxia in the metastatic cascade. We used a timer strategy based on the combination of two reporter genes, regulated by an HIF-dependent promoter, with different degradation half-lives. We

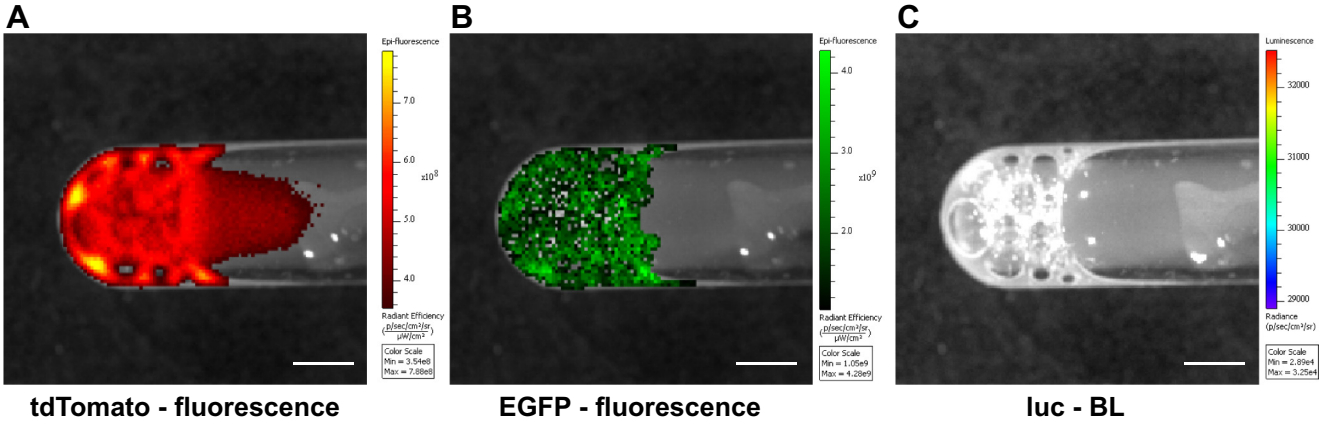

Figure 5. Representative images of cancer cells in ascites fluid obtained from the peritoneal cavity of a mouse with an orthotopic PC3-HRE-EGFP/HRE-ODD-luc/tdTomato tumor. Optical images are from (A) tdTomato expression to identify cancer cells, (B) HRE-driven EGFP expression, and (C) HRE-driven luc expression. Scale bar: 0.5 cm.

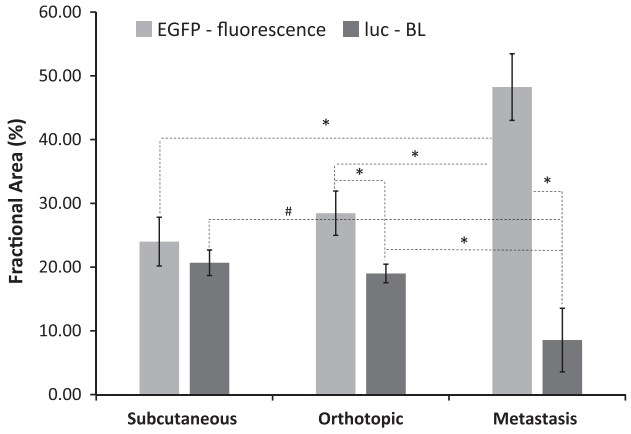

Figure 6. Bar plot displaying fractional areas of EGFP and luc expression in subcutaneous and orthotopic tumors and in metastatic nodules. Significantly higher fractional areas of EGFP fluorescence and significantly lower fractional areas of BL area were observed in metastatic lesions compared to primary tumors, suggesting that cells in metastatic lesions had been previously exposed to hypoxia either at the primary tumor site or at the metastatic site but the hypoxia had resolved. Within the groups, orthotopic tumors and metastatic lesions had significantly higher EGFP fluorescing areas compared to BL areas. Values represent mean +/- SEM from subcutaneous tumors ($n = 3$), orthotopic tumors ($n = 5$), and 15 metastatic nodules obtained from 3 orthotopic mice ($n = 3$). *Two-tailed t test, #1-tailed t test, $P < .05$.

previously established that EGFP has a degradation half-life of approximately 15 hours, while ODD-luc has an approximate half-life of 34 minutes [25]. We also previously established that luc significantly increased within 4 hours of exposure to 1% O_2, whereas EFGP significantly increased between 8 and 24 hours of exposure to 1% O_2 [25]. The combination of a long-lived EGFP and a short-lived luciferase fused to ODD allowed the identification of normoxic (EGFP–/luc–), hypoxic (EGFP+/luc+ or EGFP–/luc+), and reoxygenated (EGFP+/luc–) tumor microenvironments. Patterns of expression of the two reporters allowed us, for the first time, to evaluate hypoxia within the primary and metastatic sites of these xenografts.

We identified all four patterns of EFGP and luc expression in the primary and metastatic tumors. When we characterized the fractional area of EFGP and luc expression, we did not detect significant differences between subcutaneous and orthotopic tumors even though orthotopic PC-3 tumors are more metastatic than subcutaneous PC-3 tumors [2,26,27]. This is similar to our previous observations where we did not detect significant differences in HRE-driven EGFP expression between subcutaneous and orthotopic tumors, suggesting that hypoxia alone did not drive metastasis [26]. We have previously found that denser collagen 1 fibers and increased numbers of cancer associated fibroblasts are closely associated with a PCa dissemination permissive extracellular matrix [26]. The fractional area of EGFP expression was, however, significantly higher in the metastatic lesions compared to primary subcutaneous or orthotopic tumors, and the fractional area of luc expression was significantly lower in the metastatic lesions compared to primary subcutaneous or orthotopic tumors. Based on the half-lives of EGFP and luc (15 hours *versus* 34 minutes) and the hypoxia response times of EFGP and luc (8–24 hours *versus* 4 hours), these data suggest that cancer cells in the metastatic site were previously exposed to hypoxia. Since the fractional area of BL was significantly lower at the metastatic site, this suggests that these cancer cells may have been exposed to hypoxia at the primary site but not at the metastatic site.

Hypoxia alone was not sufficient to create a metastasis permissive environment (schematic in Figure 7*A*) since both chronic and acute

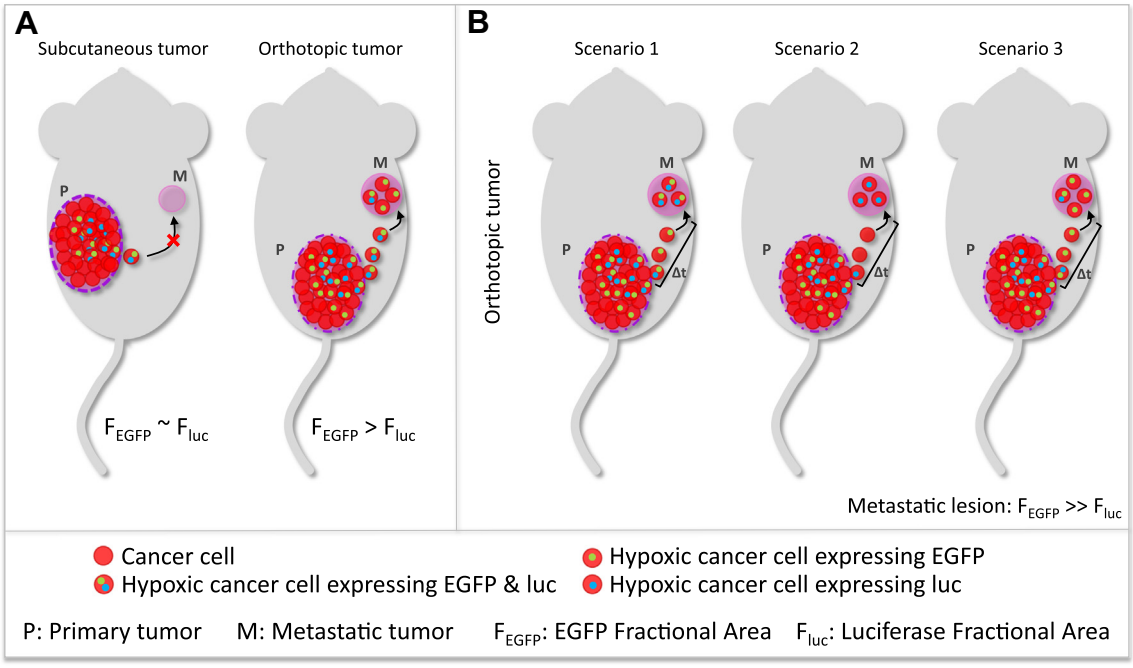

Figure 7. Schematic display of combinations of EGFP fluorescence and luc BL in primary tumors and metastatic sites and their interpretation. (A) Patterns of EGFP fluorescence and luc BL were comparable between nonmetastatic subcutaneous tumors and metastatic orthotopic tumors, indicating that there were barriers to prevent cells from leaving the primary subcutaneous tumors but these barriers were reduced in the orthotopic site. (B) In metastatic lesions from the orthotopic site, scenario 3 was the most prevalent.

hypoxic areas were not significantly different between primary tumor sites that are preventive (subcutaneous) or permissive (orthotopic) for metastasis. However, within groups, EGFP areas were significantly higher compared to BL areas in orthotopic tumors that metastasized as well as in metastatic sites. The significantly higher areas of EGFP compared to BL in orthotopic compared to subcutaneous tumors suggests that reoxygenation and the ability to reoxygenate may contribute to a metastasis permissive environment.

In metastatic sites, there was a four-fold difference between EGFP and BL fractional areas, suggesting that a high fraction of cells had been previously exposed to hypoxia. This could have been due to efficient reoxygenation occurring at the metastatic site or reoxygenated cells from the primary site continuing to seed the metastatic site. Repetitive cycles of hypoxia and reoxygenation have been previously observed to increase tumorigenicity in breast cancer cells [28]. Malignant ascites, although rare, is one complication that arises in advanced PCa from peritoneal metastasis. We found a similar pattern of high EGFP expression, but not luc, in cancer cells detected in ascites fluid, again suggesting that these cells had been exposed to hypoxia but had reoxygenated when shed into the peritoneal cavity.

The results suggest that reoxygenation in the primary tumor may result in a metastasis-permissive environment, as shown in the schematic in Figure 7*B*. The transcriptional regulation of several genes is modified by HIF, many of which are known to play a role in PCa invasion and metastasis [29,30], once the avenues to metastasize, including the vasculature and a permissive extracellular matrix, are available [26,31]. Hypoxia may also increase detachment of cells from the extracellular matrix [32] that may have played a role in the patterns observed in malignant ascites.

The limitations of our study were that we could only report on hypoxia through HIF stabilization and were not able to quantify oxygen tensions. Also, fluorescence from EGFP and BL from luc have different depths of attenuation. We therefore excised the lesions and performed imaging on 2-mm slices to quantify differences in fractional areas of EGFP fluorescence and BL. The patterns of reporter expression allowed us to confirm, for the first time, the presence of hypoxia in metastatic as well as primary lesions. While hypoxia is known to play an important role in invasion and metastasis, two critical questions are whether metastatic dissemination occurs from hypoxic primary tumor regions or if distant sites that attract metastatic cancer cells are hypoxic. Our data with this model system suggest that hypoxia followed by reoxygenation may result in a more metastatic phenotype and that hypoxia alone is not sufficient to permit metastasis. Our data support targeting hypoxia to potentially prevent metastatic dissemination from primary tumors. Development of timer proteins that provide better temporal resolution and faster response to stimuli is important to further delineate the role of hypoxia in metastatic dissemination.

Supplementary data to this article can be found online at https://doi.org/10.1016/j.neo.2018.12.004.

References

[1] Gilkes DM and Semenza GL (2013). Role of hypoxia-inducible factors in breast cancer metastasis. *Future Oncol* **9**, 1623–1636.

[2] Penet MF, Chen Z, and Bhujwalla ZM (2011). MRI of metastasis-permissive microenvironments. *Future Oncol* **7**, 1269–1284.

[3] Semenza GL (2010). Defining the role of hypoxia-inducible factor 1 in cancer biology and therapeutics. *Oncogene* **29**, 625–634.

[4] Gilkes DM, Semenza GL, and Wirtz D (2014). Hypoxia and the extracellular matrix: drivers of tumour metastasis. *Nat Rev Cancer* **14**, 430–439.

[5] Fraga A, Ribeiro R, Principe P, Lopes C, and Medeiros R (2015). Hypoxia and prostate cancer aggressiveness: a tale with many endings. *Clin Genitourin Cancer* **13**, 295–301.

[6] Hompland T, Hole KH, Ragnum HB, Aarnes EK, Vlatkovic L, Lie AK, Patzke S, Brennhovd B, Seierstad T, and Lyng H (2018). Combined MR imaging of oxygen consumption and supply reveals tumor hypoxia and aggressiveness in prostate cancer patients. *Cancer Res* **78**, 4774–4785

[7] Stewart GD, Gray K, Pennington CJ, Edwards DR, Riddick AC, Ross JA, and Habib FK (2008). Analysis of hypoxia-associated gene expression in prostate cancer: lysyl oxidase and glucose transporter-1 expression correlate with Gleason score. *Oncol Rep* **20**, 1561–1567.

[8] Ambrosio MR, Di Serio C, Danza G, Rocca BJ, Ginori A, Prudovsky I, Marchionni N, Del Vecchio MT, and Tarantini F (2016). Carbonic anhydrase IX is a marker of hypoxia and correlates with higher Gleason scores and ISUP grading in prostate cancer. *Diagn Pathol* **11**, 45.

[9] Fernandez EV, Reece KM, Ley AM, Troutman SM, Sissung TM, Price DK, Chau CH, and Figg WD (2015). Dual targeting of the androgen receptor and hypoxia-inducible factor 1alpha pathways synergistically inhibits castration-resistant prostate cancer cells. *Mol Pharmacol* **87**, 1006–1012.

[10] Milosevic M, Warde P, Menard C, Chung P, Toi A, Ishkanian A, McLean M, Pintilie M, Sykes J, and Gospodarowicz M, et al (2012). Tumor hypoxia predicts biochemical failure following radiotherapy for clinically localized prostate cancer. *Clin Cancer Res* **18**, 2108–2114.

[11] Vergis R, Corbishley CM, Norman AR, Bartlett J, Jhavar S, Borre M, Heeboll S, Horwich A, Huddart R, and Khoo V, et al (2008). Intrinsic markers of tumour hypoxia and angiogenesis in localised prostate cancer and outcome of radical treatment: a retrospective analysis of two randomised radiotherapy trials and one surgical cohort study. *Lancet Oncol* **9**, 342–351.

[12] Dunning WF (1963). Prostate cancer in the rat. *Natl Cancer Inst Monogr* **12**, 351–369.

[13] Isaacs JT, Isaacs WB, Feitz WF, and Scheres J (1986). Establishment and characterization of seven Dunning rat prostatic cancer cell lines and their use in developing methods for predicting metastatic abilities of prostatic cancers. *Prostate* **9**, 261–281.

[14] White DA, Zhang Z, Li L, Gerberich J, Stojadinovic S, Peschke P, and Mason RP (2016). Developing oxygen-enhanced magnetic resonance imaging as a prognostic biomarker of radiation response. *Cancer Lett* **380**, 69–77.

[15] Zhao D, Ran S, Constantinescu A, Hahn EW, and Mason RP (2003). Tumor oxygen dynamics: correlation of in vivo MRI with histological findings. *Neoplasia* **5**, 308–318.

[16] Glowa C, Karger CP, Brons S, Zhao D, Mason RP, Huber PE, Debus J, and Peschke P (2016). Carbon ion radiotherapy decreases the impact of tumor heterogeneity on radiation response in experimental prostate tumors. *Cancer Lett* **378**, 97–103.

[17] Horsman MR, Mortensen LS, Petersen JB, Busk M, and Overgaard J (2012). Imaging hypoxia to improve radiotherapy outcome. *Nat Rev Clin Oncol* **9**, 674–687.

[18] Unwith S, Zhao H, Hennah L, and Ma D (2015). The potential role of HIF on tumour progression and dissemination. *Int J Cancer* **136**, 2491–2503.

[19] Vaupel P, Kelleher DK, and Thews O (1998). Modulation of tumor oxygenation. *Int J Radiat Oncol Biol Phys* **42**, 843–848.

[20] Danhier F, Danhier P, Magotteaux N, De Preter G, Ucakar B, Karroum O, Jordan B, Gallez B, and Preat V (2012). Electron paramagnetic resonance highlights that the oxygen effect contributes to the radiosensitizing effect of paclitaxel. *PLoS One* **7**, e40772.

[21] Toma-Dasu I and Dasu A (2013). Modelling tumour oxygenation, reoxygenation and implications on treatment outcome. *Comput Math Methods Med* **2013**, 141087.

[22] Hu CJ, Sataur A, Wang L, Chen H, and Simon MC (2007). The N-terminal transactivation domain confers target gene specificity of hypoxia-inducible factors HIF-1alpha and HIF-2alpha. *Mol Biol Cell* **18**, 4528–4542.

[23] Tian H, McKnight SL, and Russell DW (1997). Endothelial PAS domain protein 1 (EPAS1), a transcription factor selectively expressed in endothelial cells. *Genes Dev* **11**, 72–82.

[24] Berchner-Pfannschmidt U, Frede S, Wotzlaw C, and Fandrey J (2008). Imaging of the hypoxia-inducible factor pathway: insights into oxygen sensing. *Eur Respir J* **32**, 210–217.

[25] Danhier P, Krishnamachary B, Bharti S, Kakkad S, Mironchik Y, and Bhujwalla ZM (2015). Combining optical reporter proteins with different half-lives to detect temporal evolution of hypoxia and reoxygenation in tumors. *Neoplasia* **17**, 871–881.

[26] Penet MF, Kakkad S, Pathak AP, Krishnamachary B, Mironchik Y, Raman V, Solaiyappan M, and Bhujwalla ZM (2017). Structure and function of a prostate cancer dissemination-permissive extracellular matrix. *Clin Cancer Res* **23**, 2245–2254.

[27] Penet MF, Pathak AP, Raman V, Ballesteros P, Artemov D, and Bhujwalla ZM (2009). Noninvasive multiparametric imaging of metastasis-permissive microenvironments in a human prostate cancer xenograft. *Cancer Res* **69**, 8822–8829.

[28] Louie E, Nik S, Chen JS, Schmidt M, Song B, Pacson C, Chen XF, Park S, Ju J, and Chen EI (2010). Identification of a stem-like cell population by exposing metastatic breast cancer cell lines to repetitive cycles of hypoxia and reoxygenation. *Breast Cancer Res* **12**, R94.

[29] Bizzarro V, Belvedere R, Migliaro V, Romano E, Parente L, and Petrella A (2017). Hypoxia regulates ANXA1 expression to support prostate cancer cell invasion and aggressiveness. *Cell Adh Migr* **11**, 247–260.

[30] Chen H, Chen Q, and Luo Q (2016). Expression of netrin-1 by hypoxia contributes to the invasion and migration of prostate carcinoma cells by regulating YAP activity. *Exp Cell Res* **349**, 302–309.

[31] Bhujwalla ZM, Artemov D, Natarajan K, Ackerstaff E, and Solaiyappan M (2001). Vascular differences detected by MRI for metastatic versus nonmetastatic breast and prostate cancer xenografts. *Neoplasia* **3**, 143–153.

[32] Fitzpatrick TE and Graham CH (1998). Stimulation of plasminogen activator inhibitor-1 expression in immortalized human trophoblast cells cultured under low levels of oxygen. *Exp Cell Res* **245**, 155–162.